

Sub-Doppler cooling of bosonic strontium in a two-color MOT

Milán János Negyedi, Shubha Deutschle, Florian Jessen, József Fortágh, and Lőrinc Sárkány
*Physikalisches Institut, Eberhard Karls Universität Tübingen,
Auf der Morgenstelle 14, D-72076 Tübingen, Germany*

We report a two-color magneto-optical trap that continuously operates on the $(5s^2)^1S_0 - (5s5p)^1P_1$ and $(5s5p)^3P_2 - (5s5d)^3D_3$ transitions in ^{88}Sr . Owing to the sub-Doppler cooling from the metastable $(5s5p)^3P_2$ state, a bimodal momentum distribution is observed, with the cold part of the ensemble reaching a temperature of $105\ \mu\text{K}$. A detailed simulation is established to explain the data. The absolute frequency of the $(5s5p)^3P_2 - (5s5d)^3D_3$ transition is measured to be $603\,976\,473 \pm 2\ \text{MHz}$ using a frequency comb, improving the literature value. The accompanying magnetic trap is characterized, and is shown to contribute to the sequential production of ensembles with temperatures down to $45\ \mu\text{K}$.

I. INTRODUCTION

Optical lattice clocks are a cornerstone of quantum metrology, redefining the accuracy of time and frequency standards, offering improvements in commercial applications such as GNSS systems [1–3], telecommunication [4], chronometric levelling [5], and earthquake forecasting [6], as well as tackling fundamental problems in physics, such as testing general relativity [7], dark matter research [8, 9], gravitational wave detection [10, 11], or variations in physical constants [12, 13].

A major limitation of their performance is the Dick effect that is a direct consequence of the standard, cyclic operation principle of the clock [14, 15]: alkaline-earth atoms typically have to be cooled on multiple transitions, subsequently, in order to reach the necessary μK temperatures, and are discarded after the interrogation. This leads to an effective downconversion of the phase noise of the clock laser into lower frequency regime, compromising the clock stability.

Various ideas have been proposed and demonstrated to mitigate this effect, such as dead-time free operation by combining two separate clock systems [16–18], non-destructive measurements [19, 20], or reusing the same atoms by recooling them after a spectroscopy cycle has been completed [21].

Continuously operated clocks may offer a simpler alternative route to suppress the Dick effect, therefore continuous preparation of ultracold alkaline-earth atoms is of utmost importance. Recently, continuous sources of ultracold strontium atoms have been demonstrated based on the $(5s^2)^1S_0 - (5s5p)^1P_1$ and $(5s^2)^1S_0 - (5s5p)^3P_1$ [22, 23], as well the on the $(5s5p)^3P_2 - (5s4d)^3D_3$ transition [24].

In this paper we investigate the feasibility of a single-step, continuous source of ultracold strontium atoms based on a MOT operated on the *green* $(5s5p)^3P_2 - (5s5d)^3D_3$ transition, loaded directly from a dispenser instead of using a Zeeman-slower, reducing system size and complexity. To the best of our knowledge, we have achieved the lowest reported temperature on this transition, cold enough that the atoms can be efficiently transferred into an optical dipole

trap. A detailed treatment is provided to explain the observed bimodal momentum distribution of the atoms. We have determined the absolute frequency of the $(5s5p)^3P_2 - (5s5d)^3D_3$ transition using a frequency comb, improving the literature value [25]. The measured frequency is $603\,976\,473 \pm 2\ \text{MHz}$.

Furthermore, the linear magnetic trap created by the MOT quadrupole coils is investigated, and is shown to aid in the sequential generation of atomic ensembles down to $45\ \mu\text{K}$, with populations of more than 20 thousand atoms.

II. TWO-COLOR MOT

Using the *green* $(5s5p)^3P_2 - (5s5d)^3D_3$ strontium transition for cooling has been considered several times in the literature [25, 26]. The idea behind it is to benefit from electrons being shelved into the metastable $(5s5p)^3P_2$ state while the *blue* MOT on the $(5s^2)^1S_0 - (5s5p)^1P_1$ transition is being operated, allowing concurrent operation of the blue and green cooling transitions, lowering the temperature of the trapped atoms. Additionally, since the $(5s5p)^3P_2$ state, in contrast to the $(5s^2)^1S_0$ ground state, does have quasi-degenerate substates, sub-Doppler cooling [27] is possible to occur even for the bosonic Sr isotopes, enhancing cooling even further.

The green transition is not completely cycling, atoms are lost to the $(5s5p)^3P_1$ state through various channels, as seen in Fig. 1, therefore it is unfavorable for laser cooling [25] in itself. The *mid-infrared* or *MIR* $(5s5p)^3P_2 - (5s4d)^3D_3$ transition does not suffer from the same problem (it is completely closed), therefore it was considered the preferable alternative, especially given the much lower Doppler (T_D) and recoil (T_r) temperature limits: $T_{D,g} = 230\ \mu\text{K}$, $T_{r,g} = 0.23\ \mu\text{K}$, in contrast to $T_{D,MIR} = 1.4\ \mu\text{K}$, $T_{r,MIR} = 0.013\ \mu\text{K}$ [28]. The $2.9\ \mu\text{m}$ wavelength of the mid-infrared transition presents its own unique challenges however, and so far there are only a few reports on the realization of such a MOT [28, 29].

Recently, it has been demonstrated that with some modification of the cooling scheme, the green transition

of the quadrupole. The dispensers are operated continuously, increasing the pressure to $4 \cdot 10^{-10}$ mbar. The hot atoms are prevented from directly hitting atoms in the MOT volume by a shielding wire.

According to the literature, this setup is the first one where direct loading of a 3D-MOT from a dispenser without any kind of precooling was successfully implemented for strontium. This significantly reduces experimental complexity, allowing for a compact design, and paves the way for miniaturized, transportable systems. When using the green transition as a repumper, the resulting *blue* MOT can be routinely loaded with 1.5 million atoms, we measure an atomic flux of $\Phi_{disp} = 3.0 \cdot 10^6 \pm 1.5 \cdot 10^5$ 1/s with a two-body loss rate of $\beta_b = 1.65 \cdot 10^{-6} \pm 3 \cdot 10^{-8}$ 1/s.

B. Characterization of the green MOT

Owing to the degeneracy of the $(5s5p) \ ^3P_2$ state, $\sigma^+ - \sigma^-$ sub-Doppler cooling is taking place concurrently upon operating the green MOT, as confirmed by a recent experiment [28]. Numerical simulations have shown that for an arbitrary set of parameters typically neither the density, nor the momentum of the atoms will follow a Gaussian distribution [31–34]. During the measurements presented below, the *blue* cooling beam intensity was kept at 9 mW/cm^2 , and its detuning at 51 MHz. The repumper beams were kept at maximum intensity and on resonance. All intensities given are single-beam intensities. All presented data refers to the green MOT and the atomic ensemble it generates, unless specifically noted otherwise.

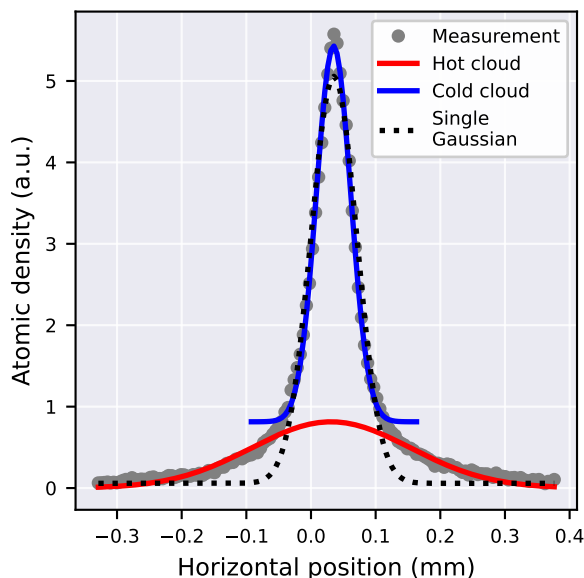


FIG. 3. Measured horizontal density distribution in the green MOT, and a comparison between fitting with one or two Gaussians. $I/I_{\text{sat}} = 0.4$, $\Delta = 1.9 \Gamma$, $G=57 \text{ G/cm}$

The density distribution of the cloud, integrated over the vertical axis, is plotted in Fig. 3 for detuning $\Delta = 1.9 \Gamma$ and a $G = 57 \text{ G/cm}$ magnetic gradient along the z -axis. It does not follow a simple Gaussian distribution: the atoms participating in the green cooling cycle separate into two distinct, overlapping clouds, suggesting two distinct components of the velocity distribution that we will label as the *cold* and the *hot* cloud. Therefore, we fit the measured atomic density profile by the sum of two Gaussians, and from this we determine the corresponding velocity distributions $F_c(v)$ and $F_h(v)$ by the usual ballistic expansion method. The velocity distribution of the entire cloud $F(v)$ is calculated as the weighted average of $F_c(v)$ and $F_h(v)$, using the respective fitted atomic populations as weights. The effective temperature of the entire cloud is defined through the expectation value of the squared velocity under $F(v)$:

$$T_{\text{eff}} = \frac{m_{\text{Sr}} \langle v^2 \rangle_F}{k_B}. \quad (1)$$

The effective temperature of the MOT is plotted as a function of the cooling intensity in Fig. 4, along with the temperature of the cold and hot fractions of the cloud, and the Doppler limit of the green transition. The lifetime of atoms in the green cooling cycle of the MOT was measured by turning off the blue cooling beams, thereby preventing it from loading. Although direct capture of a very small quantity of atoms into the green cooling cycle is theoretically possible, it is below the detection limit of our system, and was therefore neglected. The data is shown in Fig. 5, while the populations of the two clouds and the ratio of the sub-Doppler cooled atoms are shown in Fig. 6.

The MOT consistently produces a cold population with a temperature below $140 \mu\text{K}$, well below the Doppler limit of the green transition for a broad range of parameters. The coldest temperature reached is $105 \pm 9 \mu\text{K}$. This temperature is comparable to [24], despite the fact that a different transition is used, and is sufficiently low so that atoms can be efficiently loaded into an optical dipole trap or to a moving optical lattice. We have in fact loaded up to 9×10^3 atoms into a dipole trap operated at 1064 nm with $30 \mu\text{m}$ beam waist and 5 W of power, and measured a lifetime of 600 ms . This is in good agreement with the lifetime measured in the magnetic trap (see Sec. III), confirming that it is limited by background gas and Sr collisions.

We have determined the absolute frequency of the $(5s5p) \ ^3P_2 - (5s5d) \ ^3D_3$ transition by performing absorption spectroscopy on the cold atoms, as shown in Fig. 7. The cooling lasers and the magnetic coils were turned off 1 ms before imaging to eliminate Zeeman and light shifts. There are no eddy currents $500 \mu\text{s}$ after the trigger signal for turning off the coils, as confirmed by a current clamp.

The frequency of the fundamental mode of the cooling laser has been measured by beating it with a frequency comb (Toptica DFC CORE+ with DFC SCIR extension

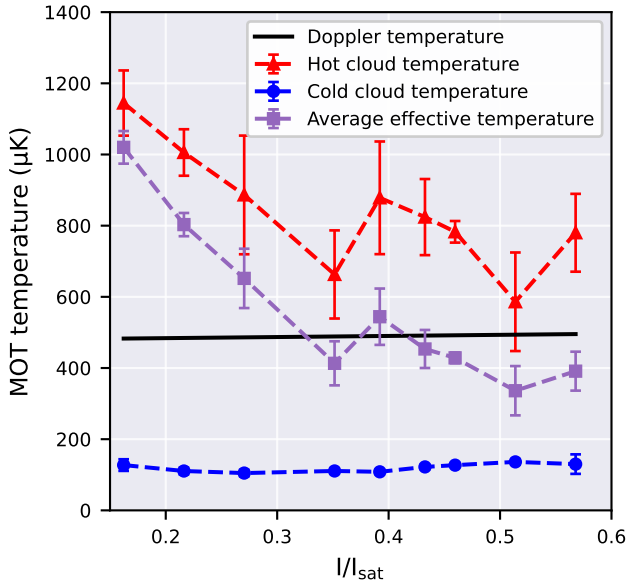


FIG. 4. Measured temperatures of the *hot* (red) and *cold* (blue) clouds, and the calculated effective temperature of total green MOT population as a function of green cooling laser intensity. $\Delta = 1.9\Gamma$, $G = 57$ G/cm

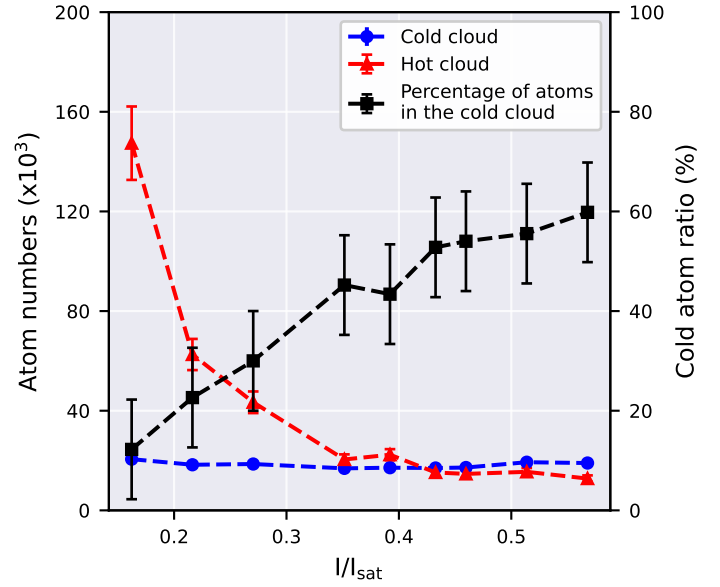


FIG. 6. Atom numbers in the *hot* (red) and *cold* (blue) cloud, and fraction of the cold atoms compared to the total atom number in the green MOT (black) as a function of green cooling laser intensity. $\Delta = 1.9\Gamma$, $G = 57$ G/cm

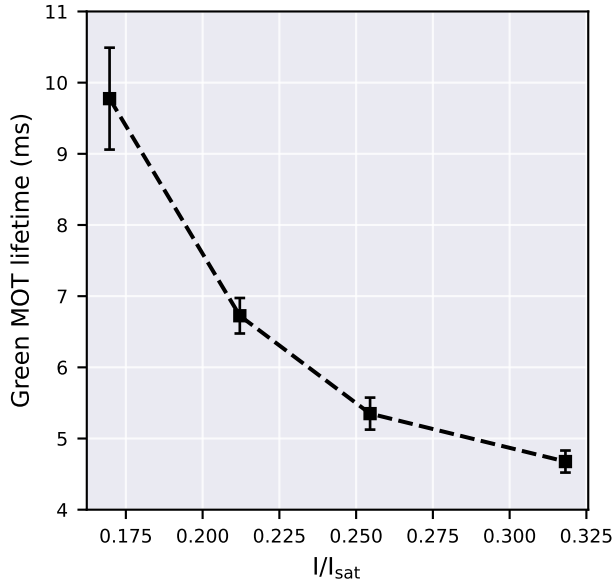


FIG. 5. The lifetime of atoms in the green cooling cycle as a function of green cooling laser intensity. $\Delta = 1.9\Gamma$, $G = 57$ G/cm

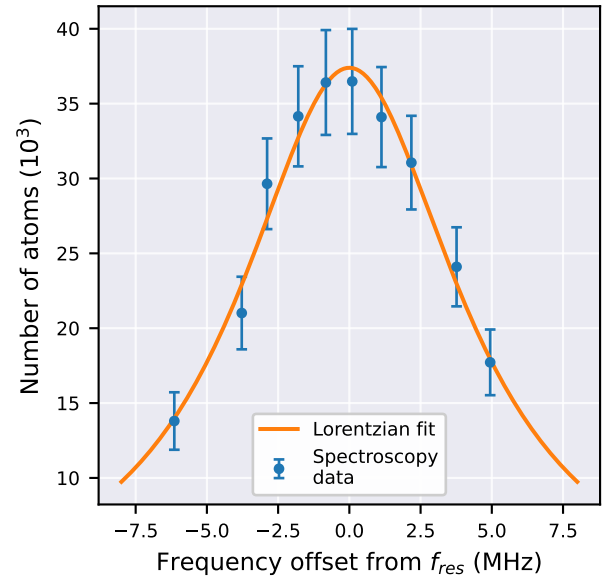


FIG. 7. Absorption spectroscopy of the green transition. $f_{\text{res}} = 603\,976\,473 \pm 2\text{MHz}$

module, 80 MHz repetition rate) that is referenced to a GPS-disciplined rubidium frequency standard (Precision Test Systems GPS10RBN).

The comb has an absolute frequency error of ~ 3 kHz, limited by the instability of the RF reference. The AOMs used to shift the green frequency back towards res-

onance are controlled by a waveform generator (Rigol DG4102), while the beat frequency was measurement by a spectrum analyzer (Signal Hound BB60C). Considering the error of the Lorentzian fit, the various instrument errors and the Zeeman shift resulting from the Earth's magnetic field, we estimate the total absolute error to be less than 2 MHz. As such, we determine the transi-

tion frequency to be $f_{\text{res}} = 603\,976\,473 \pm 2$ MHz, in slight disagreement with [25].

C. Quantum treatment of sub-Doppler cooling

Following [35], we have performed detailed numerical simulations to provide a theoretical explanation of the observed momentum distribution and effective temperature. We consider a one-dimensional problem along the z axis with two counterpropagating laserbeams with σ^+/σ^- polarizations, respectively.

As a first approximation, we neglect the effects of the magnetic fields in the MOT, considering only optical molasses. Working in two-point coordinate representation $\hat{\rho}(z_1, z_2) = \langle z_1 | \hat{\rho} | z_2 \rangle$, and changing into the coordinate system rotating along with the polarization of the total light field, the time evolution of the density matrix is described by the following equation:

$$2\omega_r \partial_q [\hat{J}_z, \hat{\rho}(q)] = \hat{\Gamma} \{ \hat{\rho}(q) \} + i\Delta \left[\hat{P}^e, \hat{\rho}(q) \right] + i\Omega \left(\hat{V}_1(q) \hat{\rho}(q) - \hat{\rho}(q) \hat{V}_2(q) \right), \quad (2)$$

subjected to normalization $\text{Tr} \hat{\rho}(q = 0) = 1$, where $q = k(z_1 - z_2)$ is the dimensionless relative coordinate, $k = 2\pi/\lambda$, $\omega_r = \hbar k^2/2M$ with M the atomic mass, $\hat{\Gamma}$ is the spontaneous atomic relaxation operator, as defined in Eq. (16) and Eq. (17) in [35], and $\Omega \hat{V}_1(q) = \Omega \hat{V}_2^\dagger(q)$ is the atom-light interaction with Rabi frequency Ω , Δ is the detuning, and

$$V_1(q) = \hat{T}_{-1} e^{-iq/2} - \hat{T}_{+1} e^{iq/2} + \text{h.c.}, \quad (3)$$

with

$$\hat{T}_\sigma = \sum_{m_e, m_g} C_{J_g, m_g; 1\sigma}^{J_e, m_e} |J_e, m_e\rangle \langle J_g, m_g|. \quad (4)$$

The results are depicted in Fig. 8.

Although this simple optical molasses calculation does already explain the non-Gaussian distribution of momentum, it fails to exactly reproduce the measured dependence on cooling power. Similarly to [31], this can be attributed to the fact that the effect of the magnetic field in the MOT can only be neglected if

$$\frac{1}{\hbar} \mu_B g_J B < \frac{\Gamma s}{1 + s + \left(\frac{2\Delta}{\Gamma}\right)^2}, \quad (5)$$

a condition which is violated in our case.

To estimate the effect of the magnetic field, we have followed the method outlined in [31]. We note that for the parameter range we have covered, the movement of the atoms in the MOT can be considered adiabatic, i.e. the trap frequency is much smaller than the cooling rate,

therefore at a given position z the equilibrium momentum distribution is determined by the local magnetic field. This allows us to approximate the total momentum distribution as a weighted average of the partial contributions originating from the subensembles of the cloud distributed along the z axis, weighted by the experimentally determined density distribution. The results of this calculation are shown in Fig. 8 under "Full quantum treatment".

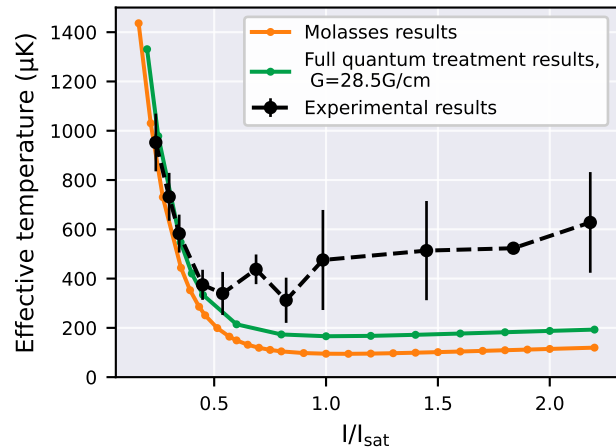


FIG. 8. The results of the full quantum treatment for a molasses and for a MOT compared with the experimental effective temperature results, as a function of green cooling laser intensity

The approximative calculation correctly predicts that the plateau of the effective temperature occurs at a higher temperature than for the molasses (Fig. 8). The optimal density and temperature of the cold cloud is reached for a saturation parameter between 0.25-0.5 (see Fig. 4) where this model already shows reasonable agreement with the measurements. For higher intensities the discrepancy between the measured and the predicted temperatures is more pronounced, suggesting that a self-consistent quantum treatment is necessary to explain the observed data. This will be the subject of a future work.

III. MAGNETIC TRAP

In the absence of cooling light, the quadrupole field of the MOT coils forms a linear magnetic trap (MT) for the low-field seeking Zeeman substates of the $(5s5p)^3P_2$ state. Typical gradients used for the MOT (45 – 60 G/cm) are sufficient to hold the atoms against gravity [36]. In our experiment, we have investigated the loading of the sub-Doppler cooled ensemble into the magnetic trap by turning off the cooling beams and observed a reduction of the temperature after the atoms have been transferred to the MT. Transfer efficiency of the cold cloud atoms to the MT was 60 percent. We have measured a lifetime of $\tau \approx 0.52$ s, limited mainly by collisions

with background gas and hot Sr atoms. The cooling effect upon transferring to the magnetic trap could open up additional possibilities for continuous preparation of the atoms based on the principles outlined in [37–39], using the magnetic field to transport and buffer the sequentially produced cold atoms for continuous loading into an optical lattice.

Due to the low atom number and shallow magnetic potential, at flight times higher than 1 ms the signal-to-noise ratio is prohibitively low for using the standard ballistic expansion method. This is compounded by the fact that the starting distribution of the MT is not Gaussian. Therefore we have used the technique described in [36] to evaluate the temperature of the cloud instead. Having calibrated the magnetic field of the coils allows us to calculate the density distribution in the trap potential, with only the temperature and the atom number as fitting parameters. Integrating the distribution along the axis of the imaging beam (y), we obtain the fitting function:

$$F(x, z, T, n_0) = n_0 \cdot \exp\left(-\frac{m_J \mu_B g_J B(x, z) - mgz}{k_B T}\right), \quad (6)$$

where $g_J = 3/2$ for the $(5s5p) \ ^3P_2$ state, and n_0 is the 2D optical density amplitude.

Since the magnetic trap is populated mainly from the cold cloud, overwhelming majority of the atoms will be in the $m_J = +2$ state, therefore we have assumed $m_J = +2$ across the whole sample. Using this method, we consistently measure temperatures T_{MT} between 45 and 60 μK in the magnetic trap, largely independent of the MOT beam intensity, significantly colder than the cold cloud of the MOT, see Fig. 9. The lowest temperature in the MT we have achieved is 44(5) μK . According to the available literature, this is the lowest value reported for strontium in a magnetic trap loaded from a MOT.

The temperature change when transferring atoms to the MT from the MOT can be estimated in an independent way using the virial theorem [40]: since the MT potential is linear, the virial theorem ensures that $V_{MT} = 2E_{MT}$, where E_{MT} and V_{MT} is the average kinetic and potential energy of the atoms in the MT, respectively. Assuming a negligible-sized MOT would lead to $E_{MOT} = E_{MT} + V_{MT} = 3E_{MT}$, i.e. $T_{MT} = T_{MOT}/3$. The finite size of the MOT slightly modifies this result to

$$T_{MT} = \frac{T_{MOT}}{3} + \frac{8}{9\sqrt{2}\pi} \frac{\mu_b g_J m_J}{k_B} G\sigma, \quad (7)$$

where σ is the radius of the MOT. The results from the two methods are in agreement with each other within measurement error, as shown in Fig. 9

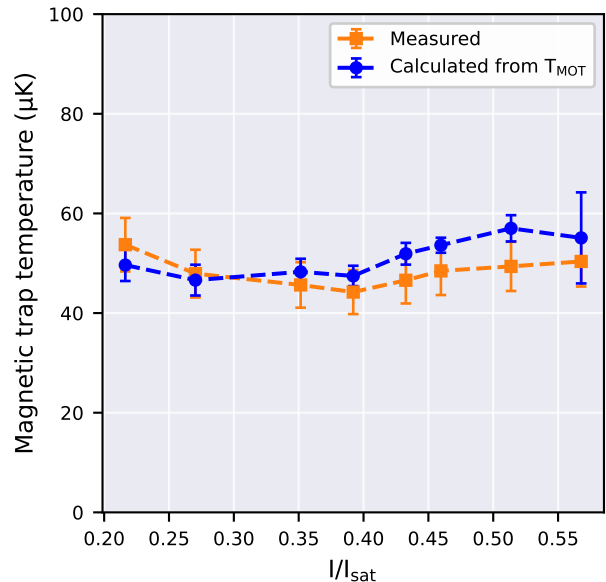


FIG. 9. T_{MT} as a function of green cooling beam intensity, as determined from absorption imaging (squares) and from T_{MOT} , using Eq. 7 (circles)

IV. CONCLUSIONS AND OUTLOOK

In this paper we have demonstrated the creation of a green strontium MOT operated on the $(5s^2) \ ^1S_0 - (5s5p) \ ^1P_1$ and $(5s5p) \ ^3P_2 - (5s5d) \ ^3D_3$ transitions, and provided a detailed theoretical and experimental analysis of the emerging momentum distribution caused by sub-Doppler cooling processes. We characterized the accompanying magnetic trap, and investigated its additional cooling effects. Our system promises to be an excellent, easy-to-realize platform to continuously source ultracold atoms with sufficient flux and temperature to be loaded into a moving optical lattice, paving the way towards continuously operated clocks and superradiant lasers.

ACKNOWLEDGMENTS

We thank H. Katori for for the joint initiation of the Strontium project, and N. Ohmae for technical consultation. The authors gratefully acknowledge financial support from the Baden-Württemberg Stiftung under project number BWST ISFIII 15, and valuable discussion with O. Prudnikov on the theoretical framework of sub-Doppler cooling. We thank C. Groß for the loan of the dipole trap laser. S Deuschle and M. Negyedi thank A. Günther for helpful discussion and advice. S. Deuschle gratefully acknowledges funding from the Vector Stiftung via project number P2023-0105.

- [1] E. Boldbaatar, D. Grant, S. Choy, S. Zaminpardaz, and L. Holden, Evaluating optical clock performance for gnss positioning, *Sensors* **23**, 10.3390/s23135998 (2023).
- [2] F. G. Major, *Quo Vadis: Evolution of Modern Navigation: The Rise of Quantum Techniques* (Springer New York, New York, NY, 2014).
- [3] T. Schuldt, M. Gohlke, M. Oswald, J. Wüst, T. Blomberg, K. Döringshoff, A. Bawamia, A. Wicht, M. Lezius, K. Voss, M. Krutzik, S. Herrmann, E. Kovalchuk, A. Peters, and C. Braxmaier, Optical clock technologies for global navigation satellite systems, *GPS Solutions* **25**, 83 (2021).
- [4] *Synchronization of Digital Telecommunications Networks* (John Wiley & Sons, Ltd, 2002) <https://onlinelibrary.wiley.com/doi/pdf/10.1002/0470845880>
- [5] J. Grotti, S. Koller, S. Vogt, S. Häfner, U. Sterr, C. Lisdat, H. Denker, C. Voigt, L. Timmen, A. Rolland, F. N. Baynes, H. S. Margolis, M. Zampaolo, P. Thoumany, M. Pizzocaro, B. Rauf, F. Bregolin, A. Tampellini, P. Barbieri, M. Zucco, G. A. Costanzo, C. Clivati, F. Levi, and D. Calonico, Geodesy and metrology with a transportable optical clock, *Nature Physics* **14**, 437 (2018).
- [6] M. Bondarescu, R. Bondarescu, P. Jetzer, and A. Lundgren, The potential of continuous, local atomic clock measurements for earthquake prediction and volcanology, in *European Physical Journal Web of Conferences*, European Physical Journal Web of Conferences, Vol. 95 (2015) p. 04009, arXiv:1506.02853 [physics.geo-ph].
- [7] M. Takamoto, I. Ushijima, N. Ohmae, T. Yahagi, K. Kokado, H. Shinkai, and H. Katori, Test of general relativity by a pair of transportable optical lattice clocks, *Nature Photonics* **14**, 411 (2020).
- [8] A. Derevianko and M. Pospelov, Hunting for topological dark matter with atomic clocks, *Nature Physics* **10**, 933 (2014).
- [9] Y. V. Stadnik and V. V. Flambaum, Searching for dark matter and variation of fundamental constants with laser and maser interferometry, *Phys. Rev. Lett.* **114**, 161301 (2015).
- [10] S. Kolkowitz, I. Pikovski, N. Langellier, M. D. Lukin, R. L. Walsworth, and J. Ye, Gravitational wave detection with optical lattice atomic clocks, *Phys. Rev. D* **94**, 124043 (2016).
- [11] G. M. Tino, A. Bassi, G. Bianco, K. Bongs, P. Bouyer, L. Cacciapuoti, S. Capozziello, X. Chen, M. L. Chiofalo, A. Derevianko, W. Ertmer, N. Gaaloul, P. Gill, P. W. Graham, J. M. Hogan, L. Iess, M. A. Kasevich, H. Katori, C. Klempt, X. Lu, L.-S. Ma, H. Müller, N. R. Newbury, C. W. Oates, A. Peters, N. Poli, E. M. Rasel, G. Rosi, A. Roura, C. Salomon, S. Schiller, W. Schleich, D. Schlippert, F. Schreck, C. Schubert, F. Sorrentino, U. Sterr, J. W. Thomsen, G. Vallone, F. Vetrano, P. Villoresi, W. von Klitzing, D. Wilkowski, P. Wolf, J. Ye, N. Yu, and M. Zhan, Sage: A proposal for a space atomic gravity explorer, *The European Physical Journal D* **73**, 228 (2019).
- [12] M. S. Safronova, S. G. Porsev, C. Sanner, and J. Ye, Two clock transitions in neutral yb for the highest sensitivity to variations of the fine-structure constant, *Phys. Rev. Lett.* **120**, 173001 (2018).
- [13] G. Barontini, L. Blackburn, V. Boyer, F. Butuc-Mayer, X. Calmet, J. R. Crespo López-Urrutia, E. A. Curtis, B. Darquié, J. Dunningham, N. J. Fitch, E. M. Forgan, K. Georgiou, P. Gill, R. M. Godun, J. Goldwin, V. Guarrera, A. C. Harwood, I. R. Hill, R. J. Hendricks, M. Jeong, M. Y. H. Johnson, M. Keller, L. P. Kozhiparambil Sajith, F. Kuipers, H. S. Margolis, C. Mayo, P. Newman, A. O. Parsons, L. Prokhorov, B. I. Robertson, J. Rodewald, M. S. Safronova, B. E. Sauer, M. Schioppo, N. Sherrill, Y. V. Stadnik, K. Szymaniec, M. R. Tarbutt, R. C. Thompson, A. Tofful, J. Tunesi, A. Vecchio, Y. Wang, and S. Worm, Measuring the stability of fundamental constants with a network of clocks, *EPJ Quantum Technology* **9**, 12 (2022).
- [14] G. J. Dick, Local oscillator induced instabilities in trapped ion frequency standards, in *Proceedings of the 19th Annual Precise Time and Time Interval Systems and Applications Meeting* (1989) pp. 133–147.
- [15] G. Santarelli, C. Audoin, A. Makdissi, P. Laurent, G. Dick, and A. Clairon, Frequency stability degradation of an oscillator slaved to a periodically interrogated atomic resonator, *IEEE Transactions on Ultrasonics, Ferroelectrics, and Frequency Control* **45**, 887 (1998).
- [16] G. W. Biedermann, K. Takase, X. Wu, L. Deslauriers, S. Roy, and M. A. Kasevich, Zero-dead-time operation of interleaved atomic clocks, *Phys. Rev. Lett.* **111**, 170802 (2013).
- [17] M. Schioppo, R. C. Brown, W. F. McGrew, N. Hinkley, R. J. Fasano, K. Beloy, T. H. Yoon, G. Milani, D. Nicolodi, J. A. Sherman, N. B. Phillips, C. W. Oates, and A. D. Ludlow, Ultrastable optical clock with two cold-atom ensembles, *Nature Photonics* **11**, 48 (2017).
- [18] E. Oelker, R. B. Hutson, C. J. Kennedy, L. Sonderhouse, T. Bothwell, A. Goban, D. Kedar, C. Sanner, J. M. Robinson, G. E. Marti, D. G. Matei, T. Legero, M. Giunta, R. Holzwarth, F. Riehle, U. Sterr, and J. Ye, Demonstration of 4.8×10^{-17} stability at 1 s for two independent optical clocks, *Nature Photonics* **13**, 714 (2019).
- [19] G. Vallet, E. Bookjans, U. Eismann, S. Bilicki, R. L. Targat, and J. Lodewyck, A noise-immune cavity-assisted non-destructive detection for an optical lattice clock in the quantum regime, *New Journal of Physics* **19**, 083002 (2017).
- [20] J. Lodewyck, P. G. Westergaard, and P. Lemonde, Non-destructive measurement of the transition probability in a sr optical lattice clock, *Phys. Rev. A* **79**, 061401 (2009).
- [21] J. P. Covey, I. S. Madjarov, A. Cooper, and M. Endres, 2000-times repeated imaging of strontium atoms in clock-magic tweezer arrays, *Phys. Rev. Lett.* **122**, 173201 (2019).
- [22] S. Bennetts, C.-C. Chen, B. Pasquiou, and F. Schreck, Steady-state magneto-optical trap with 100-fold improved phase-space density, *Phys. Rev. Lett.* **119**, 223202 (2017).
- [23] Z. Niu, V. M. Schäfer, J. R. Cline, D. J. Young, Y. Song, and J. K. Thompson, Progress toward a continuous superradiant laser, in *Optica Quantum 2.0 Conference and Exhibition* (Optica Publishing Group, 2023) p. QW3B.6.
- [24] R. Takeuchi, H. Chiba, S. Okaba, M. Takamoto, S. Tsuji, and H. Katori, Continuous outcoupling of ultracold strontium atoms combining three different traps, *Applied*

- Physics Express **16**, 042003 (2023).
- [25] S. Stellmer and F. Schreck, Reservoir spectroscopy of $5s5p\ ^3p_2$ - $5snd\ ^3D_{1,2,3}$ transitions in strontium, Phys. Rev. A **90**, 022512 (2014).
- [26] V. Schkolnik, O. Fartmann, and M. Krutzik, An extended-cavity diode laser at 497 nm for laser cooling and trapping of neutral strontium, Laser Physics **29**, 035802 (2019).
- [27] J. Dalibard and C. Cohen-Tannoudji, Laser cooling below the doppler limit by polarization gradients: simple theoretical models, J. Opt. Soc. Am. B **6**, 2023 (1989).
- [28] T. Akatsuka, K. Hashiguchi, T. Takahashi, N. Ohmae, M. Takamoto, and H. Katori, Three-stage laser cooling of Sr atoms using the $5s5p\ ^3p_2$ metastable state below doppler temperatures, Phys. Rev. A **103**, 023331 (2021).
- [29] R. Hobson, W. Bowden, A. Vianello, I. R. Hill, and P. Gill, Midinfrared magneto-optical trap of metastable strontium for an optical lattice clock, Phys. Rev. A **101**, 013420 (2020).
- [30] L. Sárkány, *Engineering quantum systems for information processing and metrology using atoms, superconductors, and light*, Ph.D. thesis, University of Tübingen (2018).
- [31] E. Kalganova, O. Prudnikov, G. Vishnyakova, A. Golovizin, D. Tregubov, D. Sukachev, K. Khabarova, V. Sorokin, and N. Kolachevsky, Two-temperature momentum distribution in a thulium magneto-optical trap, Phys. Rev. A **96**, 033418 (2017).
- [32] K. Kim, H.-R. Noh, H.-J. Ha, and W. Jhe, Direct observation of the sub-doppler trap in a parametrically driven magneto-optical trap, Phys. Rev. A **69**, 033406 (2004).
- [33] S. H. Youn, M. Lu, and B. L. Lev, Anisotropic sub-doppler laser cooling in dysprosium magneto-optical traps, Phys. Rev. A **82**, 043403 (2010).
- [34] D. P. Hansen, J. R. Mohr, and A. Hemmerich, Magnetic trapping of metastable calcium atoms, Phys. Rev. A **67**, 021401 (2003).
- [35] O. N. Prudnikov, D. V. Brazhnikov, A. V. Taichenachev, V. I. Yudin, A. E. Bonert, R. Y. Il'enkov, and A. N. Goncharov, Quantum treatment of two-stage sub-doppler laser cooling of magnesium atoms, Phys. Rev. A **92**, 063413 (2015).
- [36] S. B. Nagel, C. E. Simien, S. Laha, P. Gupta, V. S. Ashoka, and T. C. Killian, Magnetic trapping of metastable 3P_2 atomic strontium, Phys. Rev. A **67**, 011401 (2003).
- [37] D. Müller, D. Z. Anderson, R. J. Grow, P. D. D. Schwindt, and E. A. Cornell, Guiding neutral atoms around curves with lithographically patterned current-carrying wires, Phys. Rev. Lett. **83**, 5194 (1999).
- [38] H. Ott, J. Fortagh, G. Schlotterbeck, A. Grossmann, and C. Zimmermann, Bose-einstein condensation in a surface microtrap, Phys. Rev. Lett. **87**, 230401 (2001).
- [39] E. A. Hinds and I. G. Hughes, Magnetic atom optics: mirrors, guides, traps, and chips for atoms, Journal of Physics D: Applied Physics **32**, R119 (1999).
- [40] J. Stuhler, P. O. Schmidt, S. Hensler, J. Werner, J. Mlynek, and T. Pfau, Continuous loading of a magnetic trap, Phys. Rev. A **64**, 031405 (2001).